

Calculation of paramagnetic susceptibilities and specific heats by density-functional-crystal-field theory: PrPd_2X_3 and NdPd_2X_3 ($X = \text{Al}, \text{Ga}$)

Zhaosen Liu

Institut für Theoretische Physik, TU Dresden, D-01062 Dresden, Germany

Manuel Richter

Institut für Festkörper- und Werkstofforschung Dresden e.V., Postfach 270016, D-01171 Dresden, Germany

Martin Diviš

Department of Metal Physics, Charles University, Ke Karlovu 5, 121 16 Prague 2, Czech Republic

Helmut Eschrig

Institut für Festkörper- und Werkstofforschung Dresden e.V., Postfach 270016, D-01171 Dresden, Germany

(Received 9 April 1999)

A variant of the self-interaction corrected local spin-density approximation has been implemented and applied to compute the crystal field parameters for PrPd_2X_3 and NdPd_2X_3 ($X = \text{Al}, \text{Ga}$). The parameters were in turn used to calculate the crystal field states and levels, as well as the susceptibilities and specific heats of these compounds. Good agreement with available experimental data is found, at variance with results on the isostructural compound UPd_2Al_3 reported earlier. The anisotropic susceptibility is predicted for three of the considered compounds. [S0163-1829(99)02232-8]

I. INTRODUCTION

The discoveries of the heavy-fermion superconductor UPd_2Al_3 , in which superconductivity coexists with a large antiferromagnetically ordered uranium moment of $0.85\mu_B$,^{1,2} and the antiferromagnetic heavy fermion compound CePd_2Al_3 (Ref. 3) have inspired extensive experimental and theoretical investigations on the physical properties of the isostructural lanthanide compounds RPd_2Al_3 and RPd_2Ga_3 ($R = \text{Ce}, \text{Pr}, \text{Nd}, \text{Sm}$).⁴⁻¹⁰

Consider first the Al compounds. Ghosh *et al.*⁴ have systematically measured the resistivities and magnetic susceptibilities of the RPd_2Al_3 system including LaPd_2Al_3 . They found that the susceptibilities of the Ce, Pr, and Nd compounds in the high temperature range $100 \text{ K} \leq T \leq 300 \text{ K}$ obey the Curie-Weiss law with effective magnetic moments μ_{eff} of the lanthanide ions close to the free ion values, meaning that the $4f$ electrons are localized. CePd_2Al_3 and NdPd_2Al_3 show antiferromagnetic (AFM) ordering below 2.8 and 6.5 K, respectively.^{3,4,6} On the other hand, PrPd_2Al_3 does not show any magnetic ordering down to 1.5 K, and the value of the susceptibility becomes saturated below 15 K. From the resistivity studies, evidence is found for CePd_2Al_3 to be a Kondo system.⁴ In particular, the magnetic part of the resistivity exhibits a clear maximum at 30 K. A change of slope occurs at 6.5 K in the resistivity curve of NdPd_2Al_3 , which corresponds to the antiferromagnetic transition. The resistivity data of PrPd_2Al_3 show no anomaly down to 1.5 K. For SmPd_2Al_3 , the resistivity and magnetic susceptibility studies revealed at least two magnetic transitions at 4.3 and 12 K.⁴

Recently, Dönni *et al.* made detailed studies on the magnetic and thermodynamic properties of NdPd_2Al_3 .⁶ Five

samples were prepared, three polycrystals and two single crystals, and the measurements on their susceptibilities revealed that the Néel temperatures T_N of the samples, varying between 5.2 and 7.7 K, show a linear dependence on the lattice constant a , but not on c . This probably means that the magnetism in NdPd_2Al_3 is dominated by exchange interactions inside the hexagonal a - b plane. Antiferromagnetic ordering within the low-temperature range is confirmed by the λ shape of the specific heat and the second-order phase transition. The ordered Nd moments $\mu_{\text{ord}} = (2.28 \pm 0.07)\mu_B$ at saturation lie in the basal plane and are oriented perpendicular to the propagation vector $\mathbf{q} = (2\pi/a)[\frac{1}{2}, 0, 0]$. At the magnetic phase transition the symmetry is lowered from hexagonal to orthorhombic structure. The related lattice distortion was below experimental resolution.⁶

While the $4f$ electrons in the Ce compounds are on the verge of delocalization, they appear to be well localized for the other rare earth compounds and a crystal field (CF) model can be applied to explain the $4f$ related physical properties. For NdPd_2Al_3 the measured values of the magnetic entropy suggest that the energy separation of the two lowest-lying CF doublets is comparable to the Néel temperature.⁶ This is consistent with the observation of a strong transition at about 0.8 meV in a low temperature inelastic neutron scattering experiment.⁷ The completely assigned CF level sequence was $\Gamma_7 \rightarrow \Gamma_9^{(1)} \rightarrow \Gamma_8^{(1)} \rightarrow (\Gamma_9^{(2)}) \rightarrow \Gamma_8^{(2)}$, where the energy of the $\Gamma_9^{(2)}$ level was obtained from fitting susceptibility data. Two CF excitations have been resolved in the case of PrPd_2Al_3 .⁷

Similar investigations on the transport, magnetic, and thermodynamic properties of the Ga compounds ($R = \text{Pr}, \text{Nd}, \text{and Sm}$) were carried out by Bauer *et al.*⁸ For NdPd_2Ga_3 , powder neutron diffraction experiments were

TABLE I. Lattice constants (a and c) and characteristic properties of RPd_2Al_3 and RPd_2Ga_3 ($R=Pr, Nd$). The paramagnetic Curie temperature is denoted by θ_p .

compound	$PrPd_2Al_3$	$NdPd_2Al_3$	$PrPd_2Ga_3$	$NdPd_2Ga_3$
a (Å)	5.4524 ^a	5.4419 ^b	5.398 ^c	5.384 ^c
c (Å)	4.2102 ^a	4.2069 ^b	4.254 ^c	4.247 ^c
γ (mJmol ⁻¹ K ⁻²)	?	<20 ^b	?	<20 ^c
T_N (K)		7.7 ^b		6.5 ^c
θ_p (K)	40.4 ^a	21.8 ^a	-13 ^c	-2.8 ^c
μ_{eff} (μ_B)	3.45 ^a	3.59 ^a	3.40 ^c	3.64 ^c
μ_{ord} (μ_B)		2.28(7) ^b		1.99(4) ^c

^aReference 4.

^bReference 6.

^cReference 8.

performed at 1.5 K to establish the antiferromagnetic structure. Similar to $NdPd_2Al_3$, the magnetic moment is oriented perpendicular to the propagation vector $\mathbf{q}=(2\pi)/a[\frac{1}{2},0,0]$, and its value decreases smoothly from $1.99(4)\mu_B$ to zero when temperature increases from low temperature to $T_N=6.5$ K. On the other hand, $PrPd_2Ga_3$ does not show long-range magnetic order down to about 0.3 K. Different from $NdPd_2Al_3$, the inverse magnetic susceptibility of $NdPd_2Ga_3$ exhibits a strong negative curvature. This behavior was, however, not confirmed in new experiments of the same group.¹¹ In accordance with the susceptibility and the neutron scattering data, the typical λ -shaped anomaly in the specific heat of $NdPd_2Ga_3$ indicates a magnetic transition at $T_N=6.5$ K. A very characteristic temperature dependence of the electrical resistivity is found for $PrPd_2Ga_3$: above 0.35 K, the resistivity decreases with temperature, yielding a minimum in the proximity of 11 K. This observation was discussed as a possible Kondo-like behavior.⁸ $SmPd_2Ga_3$ exhibits its magnetic order below $T\approx 17$ K with a probably complex structure that has not yet been resolved.⁸ More recently, direct observations of CF excitations have been reported on $PrPd_2Ga_3$ (two excitations) and on $NdPd_2Ga_3$ (three excitations).⁹

In the present investigation, single-ion $4f$ contributions to susceptibility and specific heat are evaluated in the frame of CF model calculations with parameters obtained from density functional theory. We concentrate on those systems which are dominated by single-ion properties and exhibit a simple magnetic structure. Thus we exclude both the heavy-fermion Ce compounds and the Sm compounds, where the magnetic structure is unknown and complicated. In addition, excluding Sm compounds allows us to restrict all model calculations to the $4f$ ground state multiplet. Table I summarizes some relevant properties of the considered compounds.

Similar, self-interaction corrected (SIC) local spin density approximation (LSDA) calculations were earlier carried out to obtain the crystal field parameters for UGa_2 and UPd_2Al_3 .^{12,13} The parameters were in turn used to calculate the susceptibilities and the magnetic parts of the specific heats of these compounds in the paramagnetic state. Fair agreement between calculated and experimental susceptibilities was found for $5f^2$ occupation in both compounds in the temperature range $200\text{ K}\leq T\leq 300\text{ K}$. The calculations

failed, however, to reproduce the experimental data of the susceptibility and the specific heat of UPd_2Al_3 in the low-temperature range,¹³ and only moderate agreement was found for low temperatures in the case of UGa_2 .¹² The latter result could be improved by enforcing a stronger spatial localization of the $5f$ orbitals.¹³

The aim of the present paper is twofold. (i) A SIC-LSDA variant is presented that accounts for the first Hund's rule couplings among the $4f$ electrons within the atom and provides stronger localization of the f orbitals than conventional SIC-LSDA. (ii) This variant is applied to the class of compounds at hand to demonstrate the ability of the combined density functional-crystal field theory (DF-CFT) to describe thermodynamic properties related to localized $4f$ states.

The paper is organized in the following way. The model Hamiltonian approach used to determine thermodynamic properties is explained in Sec. II. In Sec. III, the SIC-LSDA variant employed for the calculation of crystal field Hamiltonian parameters is introduced. Section IV is devoted to the discussion of the results in comparison with experiment and Sec. V gives the conclusions.

II. MODEL APPROACH TO THERMODYNAMIC PROPERTIES

For the sake of completeness we briefly derive the basic expressions used in our calculations. The low-temperature specific heat and the paramagnetic susceptibility of the considered compounds are dominated by the respective $4f$ contributions. In this section, we first give an outline of the model approach used to determine these contributions and then discuss corrections on the susceptibility due to the conduction electrons.

We start our discussion by writing down the model Hamiltonian¹⁴

$$\mathcal{H}=\sum_{i=1}^N \mathcal{H}_{\text{CF}}^{(i)}+\mathbf{H}\sum_{i=1}^N g_J\mu_B\mathcal{J}^{(i)}+\sum_{i=1}^N \mathbf{H}_{\text{ex}}^{(i)}g_J\mu_B\mathcal{J}^{(i)}+\frac{1}{2}\sum_{i=1}^N \mathbf{H}_{\text{ex}}^{(i)}\mathbf{M}^{(i)}, \quad (1)$$

with

$$\mathbf{M}^{(i)}=-g_J\mu_B\langle\mathcal{J}^{(i)}\rangle \quad (2)$$

and

$$\mathbf{H}_{\text{ex}}^{(i)}=\left(\frac{g_J-1}{g_J\mu_B}\right)^2\sum_{j\neq i}^{j\neq i} J_{ij}\mathbf{M}^{(j)}. \quad (3)$$

This mean-field model describes magnetic structures with N local moments. The Hamiltonian \mathcal{H} contains interactions with the crystal field (CF Hamiltonian, \mathcal{H}_{CF}), with a homogeneous external field \mathbf{H} (Zeeman term), and isotropic exchange coupling between the magnetic ions (third and fourth term). The latter interaction is obtained from Heisenberg-like coupling

$$-\frac{(g_J-1)^2}{2}\sum_{ij}^{i\neq j} J_{ij}\mathcal{J}^{(i)}\mathcal{J}^{(j)}, \quad (4)$$

if the molecular field approximation is applied. Here and above, $\mathcal{J}^{(i)}$ denotes the total $4f$ angular momentum operator at site i . Since exchange coupling via the conduction electrons [Ruderman-Kittel-Kasuya-Yosida (RKKY)] is the dominating mechanism, the prefactor $(g_J - 1)^2$ ensures similar values of J_{ij} for isostructural compounds with different rare earths. Note, that the notation introduced in Eq. (4) is only valid in the simple case of negligible J mixing. The thermal expectation value of the local magnetic moment at site i is called $\mathbf{M}^{(i)}$, and the transferred exchange field acting on that site, $\mathbf{H}_{\text{ex}}^{(i)}$.

We now specify the general notation according to the situations to be described. Without an external field applied, the compounds are either in a paramagnetic state with zero mean local moment or antiferromagnetic with propagation vector $\mathbf{q} = (2\pi/a)[\frac{1}{2}, 0, 0]$. Thus,

$$\mathbf{M}^{(j)} = \mathbf{M}^{(i)} e^{iq(\mathbf{R}_i - \mathbf{R}_j)} = \pm \mathbf{M}_{4f}, \quad (5)$$

where \mathbf{R}_i are site positions and \mathbf{M}_{4f} is the moment at some arbitrary site $i=0$. Consequently,

$$\mathbf{H}_{\text{ex}}^{(i)} = \left(\frac{g_J - 1}{g_J \mu_B} \right)^2 \mathbf{M}^{(i)} \sum_j^{j \neq i} J_{ij} e^{iq(\mathbf{R}_i - \mathbf{R}_j)}. \quad (6)$$

The problem separates into effective single-ion problems

$$\mathcal{H}^{\text{AFM}} = \mathcal{H}_{\text{CF}} + \mathbf{H}_{\text{ex}}^{\text{AFM}} \left(g_J \mu_B \mathcal{J} + \frac{1}{2} \mathbf{M}_{4f} \right), \quad (7)$$

$$\mathbf{H}_{\text{ex}}^{\text{AFM}} = \left(\frac{g_J - 1}{g_J \mu_B} \right)^2 \mathbf{M}_{4f} J(\mathbf{q}). \quad (8)$$

The exchange field is determined by a single parameter, the \mathbf{q} component of the Fourier transformed exchange coupling,

$$J(\mathbf{q}) = \sum_j^{j \neq 0} J_{0j} e^{iq(\mathbf{R}_0 - \mathbf{R}_j)}. \quad (9)$$

Diagonalization of \mathcal{H}^{AFM} for some given value of \mathbf{M}_{4f} (along the easy axis of magnetization, i.e., in the hexagonal plane and perpendicular to the propagation vector \mathbf{q}) yields eigenvalues ε_ν and eigenstates $|\Gamma_\nu\rangle$ within the $4f$ ground state multiplet. In turn, the $4f$ magnetization is obtained as

$$\mathbf{M}_{4f}(T) = -\mu_B g_J \sum_\nu e^{-\varepsilon_\nu(T)/k_B T} \langle \Gamma_\nu | \mathcal{J} | \Gamma_\nu \rangle / Z_{\text{eff}}, \quad (10)$$

with an effective partition function

$$Z_{\text{eff}} = \sum_\nu e^{-\varepsilon_\nu(T)/k_B T}. \quad (11)$$

The Eqs. (7),(8),(10) have to be solved self-consistently. Since we are able to find the parameters entering \mathcal{H}_{CF} from density functional calculations (next section), $J(\mathbf{q})$ is the only remaining free parameter. Its value can be obtained from the requirement that $\mathbf{M}_{4f}(T)$ should vanish at the Néel temperature of the Nd compounds. For the Pr compounds this is not a possibility because they do not order in experi-

ment. This can be attributed to the singlet ground state of Pr on the one hand, and to the small value of $(g_J - 1)^2$ on the other hand.

Having obtained the eigenvalues ε_ν and taking into account their temperature dependence for $T < T_N$, we can evaluate the magnetic contribution to the specific heat,

$$\begin{aligned} c_m &= N_A T \frac{\partial^2}{\partial T^2} (k_B T \ln Z_{\text{eff}}) \\ &= k_B N_A \left[\frac{1}{Z_{\text{eff}}} \sum_\nu e^{-\varepsilon_\nu/k_B T} \left\{ \left(\frac{\varepsilon_\nu}{k_B T} \right)^2 - \frac{\varepsilon_\nu \varepsilon'_\nu}{k_B^2 T} \right\} \right. \\ &\quad \left. - \frac{1}{Z_{\text{eff}}^2} \left\{ \sum_\nu e^{-\varepsilon_\nu/k_B T} \frac{\varepsilon_\nu}{k_B T} \right\}^2 \right]. \quad (12) \end{aligned}$$

Here, N_A denotes Avogadro's number and ε'_ν is the first derivative of ε_ν with respect to T .

Turning our attention to the susceptibility, we only consider the paramagnetic state. Now, in a small external field, the transferred exchange field is governed by $J(0)$:

$$\mathbf{H}_{\text{ex}}^{\text{PM}} = \left(\frac{g_J - 1}{g_J \mu_B} \right)^2 \mathbf{M}_{4f} J(0) \quad (13)$$

and

$$\mathcal{H}^{\text{PM}} = \mathcal{H}_{\text{CF}} + (\mathbf{H} + \mathbf{H}_{\text{ex}}^{\text{PM}}) g_J \mu_B \mathcal{J}. \quad (14)$$

The second order term in \mathbf{M}_{4f} may now be neglected. Since we do not attempt to calculate the exchange coupling $J(0)$ we restrict our further consideration to the crystal field susceptibility

$$\chi_{\text{CF}} = N_A \left. \frac{\partial \mathbf{M}_{4f}}{\partial \mathbf{H}} \right|_{H=0, H_{\text{ex}}^{\text{PM}}=0}. \quad (15)$$

This simplification only neglects a constant shift of the inverse $4f$ susceptibility by the amount of the molecular field constant,

$$\lambda = N_A \left(\frac{g_J - 1}{g_J \mu_B} \right)^2 J(0). \quad (16)$$

If we assume that the absolute value of $J(0)$ has a similar magnitude as that of $J(q)$, $|\lambda| \approx 2-5$ mol/emu for the considered systems.

Finally, valence electron contributions to the susceptibility should be included. Any ordered component of the $4f$ magnetization will induce an according valence electron magnetization with an ordered moment \mathbf{M}_c per rare earth atom of

$$\mathbf{M}_c = 2J_{f-c}(0) D(E_F) \frac{g_J - 1}{g_J} \mathbf{M}_{4f}. \quad (17)$$

Here, $J_{f-c}(0)$ defines the $4f$ -valence electron coupling constant, and $D(E_F)$ is the spin density of states at the Fermi level. Taking into account both the conduction electron polarization by the $4f$ magnetization and *vice versa*, we arrive at¹⁵

$$\chi_{\text{CF}} + \chi_{f-c} = \chi_{\text{CF}} \left[1 + 2J_{f-c}(0)D(E_F) \frac{g_J - 1}{g_J} \right]^2, \quad (18)$$

χ_{f-c} denoting the $4f$ -valence electron interaction contribution to the susceptibility. We can obtain the induced moment directly by an LSDA calculation,¹⁶ if we treat the localized $4f$ states as polarized core states^{17,18} with ferromagnetic alignment. In this way we find $2J_{f-c}(0)D(E_F) \approx 0.05$, providing a linear reduction of the susceptibility by about 4% in the considered light- R compounds. Pauli and Landau contributions can be estimated from the almost temperature independent susceptibility of LaPd_2Al_3 that amounts to 6.0×10^{-5} emu/mol.⁵ From the calculated density of states at the Fermi level we find Pauli susceptibilities of $6-8 \times 10^{-5}$ emu/mol for the compounds at hand, in good agreement with the quoted experiment. This finding justifies the neglect of Landau contributions. The Pauli susceptibility χ_P amounts to at most 4% of the total susceptibility χ , and partially compensates χ_{f-c} ,

$$\chi = \chi_{\text{CF}} + \chi_{f-c} + \chi_P. \quad (19)$$

The direction of the external field is chosen either along the hexagonal axis or perpendicular to this axis to find χ_{\parallel} and χ_{\perp} , respectively. The average susceptibility for polycrystalline samples is estimated by

$$\chi_{\text{poly}} = (\chi_{\parallel} + 2\chi_{\perp})/3. \quad (20)$$

III. DF CALCULATION OF CF MODEL HAMILTONIAN COEFFICIENTS FOR A LOCALIZED, POLARIZED f SHELL

We now concentrate on the evaluation of coefficients entering the crystal field Hamiltonian \mathcal{H}_{CF} from density functional theory. Given a localized $4f$ shell with fixed occupation, \mathcal{H}_{CF} defines the nonspherical interactions lifting the degeneracy of the $4f$ Russel-Saunders ground state multiplet $|JJ_z\rangle$. Admixture of contributions from higher multiplets is unimportant for Pr and Nd below room temperature. We have checked this fact by including $J=11/2$ and $J=13/2$ terms when calculating the susceptibility of the Nd compounds and found almost no change with respect to the calculation restricted to the $J=9/2$ ground state multiplet. Thus, all further considerations are restricted to the ground state multiplet. If we further refrain from an orthorhombic distortion that may occur (but was not experimentally⁶ resolved) in the case of ordered moments oriented in the x - y plane, the CF Hamiltonian for hexagonal symmetry reads¹⁹

$$\begin{aligned} \mathcal{H}_{\text{CF}} = & \alpha_2 A_{20} \langle r^2 \rangle \mathcal{O}_{20} + \alpha_4 A_{40} \langle r^4 \rangle \mathcal{O}_{40} + \alpha_6 (A_{60} \langle r^6 \rangle \mathcal{O}_{60} \\ & + A_{66} \langle r^6 \rangle \mathcal{O}_{66}). \end{aligned} \quad (21)$$

This notation includes Stevens parameters α_l , CF coefficients A_{lm} , Stevens operators \mathcal{O}_{lm} ,²⁰ and radial expectation values

$$\langle r^l \rangle = \int dr 4\pi r^{l+2} R_{4f}^2(r), \quad \langle r^0 \rangle = 1, \quad (22)$$

with radial $4f$ wave functions R_{4f} .

The Stevens parameters are atomic quantities only depending on the $4f$ occupation and on the total angular momentum J , whereas the CF coefficients are determined by the crystal potential and the radial $4f$ density $4\pi r^2 R_{4f}^2(r)$. Spin density functional theory²¹ (SDFT) provides access to both an effective spin dependent crystal potential $v_{\sigma\sigma'}^{\text{eff}}[\mathbf{n}]$ and to the total ground state spin density matrix $\mathbf{n} = n_{\sigma\sigma'}(\mathbf{r})$; $\sigma, \sigma' = (\uparrow, \downarrow)$. The effective potential includes the spin-independent potentials of the atomic nuclei v^{nuc} and of the Hartree term. The most common implementation of SDFT is the local spin density approximation. In this approach, for a diagonal spin density matrix, the likewise diagonal exchange-correlation potential, v_{σ}^{xc} adds to the spin-independent contributions of the effective potential

$$v_{\sigma}^{\text{eff}}[\mathbf{n}](\mathbf{r}) = v^{\text{nuc}}(\mathbf{r}) + \int d^3r' \frac{n(\mathbf{r}')}{|\mathbf{r}-\mathbf{r}'|} + v_{\sigma}^{\text{xc}}[n_{\uparrow}(\mathbf{r}), n_{\downarrow}(\mathbf{r})], \quad (23)$$

$$n = n_{\uparrow} + n_{\downarrow}. \quad (24)$$

We note, that in a periodic lattice the definition of a part of the total density to be ‘‘localized $4f$ density’’ is not strictly possible in LSDA. The reason is that v^{eff} is periodic and any projection of single-particle states onto local orbitals involves some arbitrariness. A much more consistent description is possible in the frame of self-interaction corrected LSDA.^{22,23} In this scheme, the effective potential is state dependent,

$$v_{\sigma, \nu}^{\text{eff}}[\mathbf{n}; n_{\nu}] = v_{\sigma}^{\text{eff}}[\mathbf{n}] - \int d^3r' \frac{n_{\nu}(\mathbf{r}')}{|\mathbf{r}-\mathbf{r}'|} - v_{\uparrow}^{\text{xc}}[n_{\nu}(\mathbf{r}), 0]. \quad (25)$$

The correction potential vanishes for extended states ν , since in this case the related orbital density vanishes, $n_{\nu} \rightarrow 0$. It, however, destroys the translational invariance of $v_{\sigma}^{\text{eff}}[\mathbf{n}]$ for localized states. Translational invariance now means

$$v_{\sigma, \nu}^{\text{eff}}[\mathbf{n}; n_{\nu}(\mathbf{r}-\mathbf{R})](\mathbf{r}-\mathbf{R}) = v_{\sigma, \nu}^{\text{eff}}[\mathbf{n}; n_{\nu}(\mathbf{r})](\mathbf{r}). \quad (26)$$

The localization is self-stabilizing for $\nu=4f$ in most rare earth systems, but has to be initialized by a symmetry breaking potential.

Having clarified the subdivision into localized $4f$ density belonging to one specific rare earth site, and the remaining density, we can obtain the CF coefficients from the components of the effective potential in spherical harmonics representation $\tilde{v}_{lm}^{\text{eff}}$ via²⁴

$$A_{lm} \langle r^l \rangle = C_{lm} \int dr 4\pi r^2 R_{4f}^2(r) \tilde{v}_{lm}^{\text{eff}}(r), \quad (27)$$

$$C_{20} = \sqrt{\frac{5}{16\pi}}, \quad C_{40} = \sqrt{\frac{9}{256\pi}},$$

$$C_{60} = \sqrt{\frac{13}{1024\pi}}, \quad C_{66} = \sqrt{\frac{6006}{4096\pi}}. \quad (28)$$

The tilde on $\tilde{v}_{lm}^{\text{eff}}$ means that it is calculated from that self-consistent spin density $\tilde{\mathbf{n}}$ of the crystal, which is obtained if

the $4f$ charge density on the considered atom is constrained to its spherical average. Moreover, to avoid unnecessary complications, each orbital density n_{4f} is spherically averaged.²²

Two ingredients are required for the calculation of the CF coefficients according to Eq. (27): the full effective crystal potential and the radial $4f$ wave function. The former is evaluated using a method described explicitly in Ref. 25. The main issue we wish to address in this section is the correct treatment of the $4f$ states and the sensitivity of the radial $4f$ wave function to this treatment. We have shown in previous investigations^{27-29,12,30} that correction for self-interaction in the localized $4f$ shell is a consistent approach to crystal field properties. Besides the aforementioned, more formal difficulty to define which part of total density belongs to localized states, there exists a practical handicap for applying simple LSDA to localized $4f$ states.²⁷ Given a subdivision of the crystal potential into atomic site potentials v_i , an LSDA calculation of atomiclike $4f$ states within the spherical potential v_i (\mathbf{R}_i being a rare earth site) usually yields $4f$ single-particle energies ε_{4f} above the continuum edge of v_i . Thus there is no way, within LSDA, to obtain localized $4f$ states, except to introduce more or less arbitrary constraints such as atomic-sphere boundary conditions. This problem disappears if self-interaction is corrected for, bringing down ε_{4f} by roughly 10 eV for the occupied states in early lanthanides:

$$v_{i\sigma,4f}[n_{\uparrow}, n_{\downarrow}; n_{4f}] = v_{i\sigma}[n_{\uparrow}, n_{\downarrow}] - \int d^3r' \frac{n_{4f}(\mathbf{r}')}{|\mathbf{r} - \mathbf{r}'|} - v_{\uparrow}^{\text{sc}}[n_{4f}(\mathbf{r}), 0]. \quad (29)$$

We have applied this scheme both to paramagnetic states^{27,30} and to magnetically ordered states.^{28,29} In the latter case, the valence electron polarization was described in the conventional LSDA approach, and the $4f$ polarization was determined by the demand^{17,18} that the $4f$ spin moment should be equal to its Russel-Saunders value $-\mu_B 2(g_J - 1)J_z$.

The paramagnetic states, on the other hand, have been approximated by means of nonmagnetic SIC-L(S)DA calculations, correctly assuming the *mean* spin polarization to be zero, $n_{\uparrow} = n_{\downarrow} = n/2$. However, comparison of our results with experiment gave reason to the suspicion that the radial f densities were obtained too far extended even if SIC was included. This was particularly the case for $5f$ states in UGa_2 .^{12,13} In the following, we suggest a scheme that takes into account the first Hund's rule correlations present in a localized f shell also in the paramagnetic state of the crystal. This scheme provides deeper f levels and more localized f densities than nonmagnetic SIC-LSDA. It improves, as will be demonstrated for the considered class of compounds, the agreement between calculated and experimental CF levels.

It is well known that $4f$ local moments persist in the paramagnetic state, though with randomly fluctuating orientations. Hund's rules correlations are present within the $4f$ shell since the time scale of the local moment fluctuations is large in comparison to the electron orbit time.^{31,32} All $4f$ spins are parallel within one atom, in accordance with Hund's first rule, but do fluctuate in common to form the paramagnetic state. In other words, each $4f$ electron does

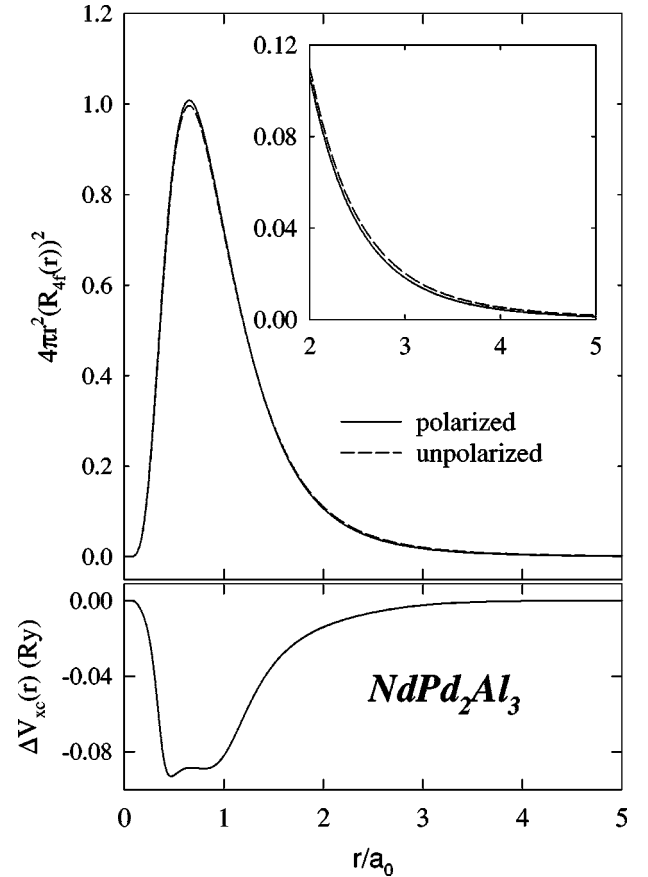


FIG. 1. Difference between unpolarized and polarized SIC-LSDA potential $\Delta v_{xc} = v_{4f} - v_{\uparrow,4f}$, according to Eq. (30) for Nd in NdPd_2Al_3 (lower part) and $4f$ radial charge density $4\pi r^2 R_{4f}^2$ for the same atom (dashed line: density of the unpolarized $4f$ shell; full line: density of the polarized $4f$ shell).

experience, at any given moment, the maximum spin polarization produced by the other electrons in the shell. The description of such dynamical correlations is beyond the scope of SDFT. In order to build in the effects of slowly fluctuating polarization on the $4f$ density into SIC-LSDA we suggest to replace the nonmagnetic potential used hitherto by its polarized equivalent

$$v_{i,4f}\left[\frac{n}{2}, \frac{n}{2}; n_{4f}\right] \rightarrow v_{i\sigma,4f}\left[\frac{n}{2} + \Delta n_{\uparrow}, \frac{n}{2} - \Delta n_{\uparrow}; n_{4f}\right], \quad (30)$$

$$\Delta n_{\uparrow} = \left(N_{\uparrow}^{4f} - \frac{N^{4f}}{2}\right) n_{4f}. \quad (31)$$

Here, N^{4f} means the total number of $4f$ electrons in the shell, and $N_{\uparrow}^{4f} = N^{4f} - N_{\downarrow}^{4f}$ the number of $4f$ electrons with majority spin direction. The difference between the dynamical (short time scale) $4f$ spin-up density $N_{\uparrow}^{4f} n_{4f}$ and the mean (long time scale) $4f$ spin-up density $N^{4f} n_{4f}/2$ is called Δn_{\uparrow} ($= -\Delta n_{\downarrow}$). Note, that we consider a situation with maximum spin polarization present

$$N_{\uparrow}^{4f} = N^{4f} \quad \text{if} \quad N^{4f} < 7; \quad \text{else} \quad N_{\uparrow}^{4f} = 7. \quad (32)$$

The difference between both potentials given in Eq. (30) is shown in Fig. 1 for the case of Nd in NdPd_2Al_3 , together

TABLE II. Comparison of radial expectation values $\langle r^l \rangle [a_0^l]$ and crystal field coefficients $A_{lm} \langle r^l \rangle$ (K) for Nd in NdPd₂Al₃ obtained by SIC-LSDA calculations with unpolarized and polarized 4*f* shell, respectively.

	Unpolarized	Polarized
$\langle r^2 \rangle$	1.39	1.33
$\langle r^4 \rangle$	7.11	6.07
$\langle r^6 \rangle$	118	87.5
$A_{20} \langle r^2 \rangle$	-475	-501
$A_{40} \langle r^4 \rangle$	77.5	57.6
$A_{60} \langle r^6 \rangle$	-4.3	3.5
$A_{66} \langle r^6 \rangle$	-288	-354

with the related 4*f* radial charge densities. In this particular case, the replacement of v_i lowers ε_{4f} by about 1 eV.

What about the treatment of valence electrons? Being itinerant, these electrons do meet polarized 4*f* shells at each rare earth site, but with randomly oriented spin quantization axes,

$$v^{\text{eff}} = \sum_i v_{i,\sigma\sigma'} [n + \Delta \mathbf{n}]. \quad (33)$$

A possible tool to describe such a situation would be the coherent potential approximation usually applied in alloy theory. Another, more reasonable description is to construct a supercell with randomly oriented moments.³³ Both these approaches are much too complicated for our purposes. Instead, we make use of the simpler virtual crystal approximation, i.e., the random potentials $v_{i,\sigma\sigma'}$ are replaced by their averaged values on each inequivalent lattice site. Taking into account the approximate linear dependence of v_{xc} on the spin polarization,²¹ the averaged randomly polarized potentials can be well approximated by the related nonmagnetic potentials $v_i[n]$.

Results on radial expectation values and CF coefficients for NdPd₂Al₃, obtained by neglecting or taking into account the polarization of the 4*f* shell, respectively, are compiled in Table II. The difference between both schemes is marginal for the second order values, but essential differences are found for fourth and sixth order. To illustrate the impact of these changes on the CF levels, we compare the level scheme obtained from both sets of coefficients with experimental CF levels⁷ in Fig. 2. The agreement between theory and experiment is definitely better for the calculation taking into account the 4*f* polarization. We have used this method for all calculations presented below.

IV. RESULTS AND DISCUSSIONS

The RPd₂X₃ compounds studied in the present work exhibit hexagonal structure at room temperature. Rare earth and Pd atoms are on the same layers, alternating along the *c* direction with pure Al or Ga layers. The lattice constants used in our calculations are given in Table I. For the PrPd₂Al₃ compound, they were extracted from a figure in Ref. 4. The lattice parameters of the NdPd₂Al₃ compound, given in Table I, were measured at room temperature.⁶ It should be mentioned that the lattice constants of this com-

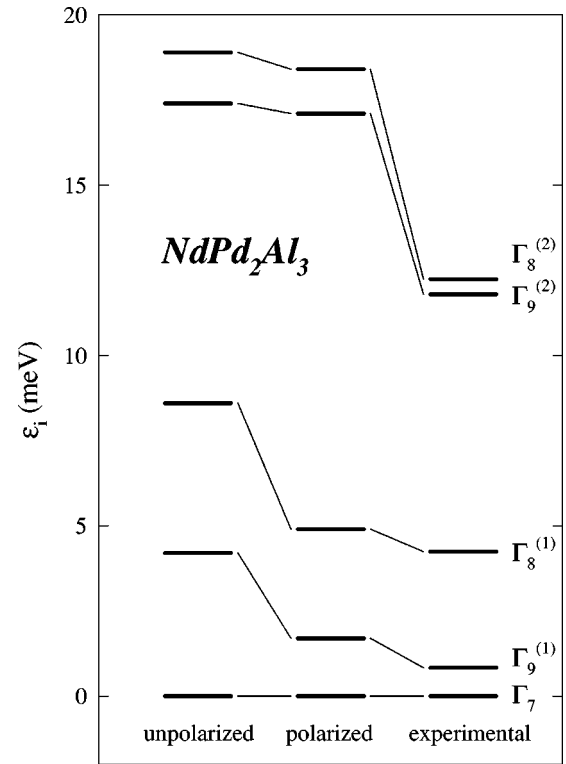


FIG. 2. Crystal field levels of NdPd₂Al₃. Left: Our calculation, unpolarized 4*f* shell; middle: our calculation, polarized 4*f* shell; right: experimental levels (Ref. 7).

pound are decreased to $a = 5.427$ Å and $c = 4.203$ Å at 14 K.⁶ This small change of the parameters does not significantly affect the properties addressed in our calculations. The lattice constants of the PrPd₂Al₃ and PrPd₂Ga₃ compounds were measured by x-ray diffraction at room temperature.⁸

With the above lattice parameters as input to the SIC-LSDA code, we obtained the moments $\langle r^l \rangle$ and $A_{lm} \langle r^l \rangle$ ($l = 2, 4, 6$) as tabulated in Table III. To compare our results with data found in literature, the CF coefficients in Table III were converted to the CF parameters $B_{lm} = \alpha_l A_{lm} \langle r^l \rangle$, and are listed in Tables IV–VII together with the corresponding crystal field levels and eigenfunctions.

Low-temperature measurements of inelastic neutron scattering (INS) (at $T = 15$ K) have shown one excitation at an energy of 5.5 meV in the case of PrPd₂Al₃.⁷ Since the CF ground state is the Γ_1 singlet, only one strong CF excitation to the Γ_5 doublet is allowed by the dipolar selection rules. Our calculated DF-CFT value is 3.1 meV which is in reason-

TABLE III. Calculated crystal field coefficients and radial moments.

Compound	PrPd ₂ Al ₃	NdPd ₂ Al ₃	PrPd ₂ Ga ₃	NdPd ₂ Ga ₃
$\langle r^2 \rangle (a_0^2)$	1.53	1.33	1.47	1.30
$\langle r^4 \rangle (a_0^4)$	8.88	6.07	7.32	5.35
$\langle r^6 \rangle (a_0^6)$	165	87.5	109	63.9
$A_{20} \langle r^2 \rangle$ (K)	-476	-501	-510	-572
$A_{40} \langle r^4 \rangle$ (K)	119	57.6	67.6	42.5
$A_{60} \langle r^6 \rangle$ (K)	-25.8	3.5	12.1	15.4
$A_{66} \langle r^6 \rangle$ (K)	38.8	-354	-604	-524

TABLE IV. CF parameters B_{lm} (meV), eigenfunctions Γ_ν , and eigenenergies ε_ν (meV) of PrPd_2Al_3 calculated by DF-CFT in comparison with the experimental (INS) or fitted and extrapolated data of Ref. 7.

B_{lm} (this work)		B_{lm} (Ref. 7)		
B_{20}	0.863	B_{20}	0.758 ± 0.018	
B_{40}	-0.752×10^{-2}	B_{40}	$(-0.312 \pm 0.006) \times 10^{-2}$	
B_{60}	-0.136×10^{-3}	B_{60}	$(0.458 \pm 0.012) \times 10^{-4}$	
B_{66}	0.204×10^{-3}	B_{66}	$(-0.894 \pm 0.043) \times 10^{-3}$	
Γ_ν (this work)	ε_ν	Γ_ν (Ref. 7)	ε_ν	
Γ_3	$0.707 +3\rangle + 0.707 -3\rangle$	$\Gamma_6^{(2)}$	$0.078 \pm 2\rangle - 0.997 \mp 4\rangle$	38.7 ± 0.7
Γ_4	$0.707 +3\rangle - 0.707 -3\rangle$	Γ_4	$0.707 +3\rangle - 0.707 -3\rangle$	30.2 ± 0.4
$\Gamma_6^{(2)}$	$0.0170 \pm 2\rangle + 0.9999 \mp 4\rangle$	Γ_3	$0.707 +3\rangle + 0.707 -3\rangle$	25.7 ± 0.3
$\Gamma_6^{(1)}$	$0.9999 \pm 2\rangle - 0.0170 \mp 4\rangle$	$\Gamma_6^{(1)}$	$0.997 \pm 2\rangle + 0.078 \mp 4\rangle$	16.82 ± 0.05^a
Γ_5	$ \pm 1\rangle$	Γ_5	$ \pm 1\rangle$	5.50 ± 0.01^a
Γ_1	$ 0\rangle$	Γ_1	$ 0\rangle$	0.0000

^aINS data.

able agreement with the value of 5.5 meV obtained from the INS data. At higher temperature, $T=40$ K, the INS spectra have shown that the strong $\Gamma_1 \rightarrow \Gamma_5$ excitation is weakened and another excitation at the 11.3 meV is observed. This second excitation was identified as $\Gamma_5 \rightarrow \Gamma_6^{(1)}$, and the related energy transfer can be compared with our calculated value of 13.1 meV. We have calculated the transition intensities of INS spectra at $T=15$ K and $T=40$ K and have found that all other transitions (e.g., $\Gamma_5 \rightarrow \Gamma_6^{(2)}$, $\Gamma_6^{(1)} \rightarrow \Gamma_4$, $\Gamma_6^{(1)} \rightarrow \Gamma_3$) should have very small intensity in comparison to that of $\Gamma_1 \rightarrow \Gamma_5$ and $\Gamma_5 \rightarrow \Gamma_6^{(1)}$. This result is in full agreement with the INS data,⁷ since they do not point to any other transitions except those mentioned above. In Ref. 7, the CF parameters for PrPd_2Al_3 were finally obtained by rescaling the fitted CF parameters for NdPd_2Al_3 with the appropriate $\alpha_l \langle r^l \rangle$ values for Nd and Pr ions. They are compared with our DF-CFT values in Table IV. Our calculated values of B_{20} and B_{40} have the same signs and same orders of magnitude as those given in Ref. 7, but B_{60} and B_{66} have different signs. Since, however, in a fitting procedure the magnitudes of B_{60} and B_{66} are sensitive to the eigenenergies

and eigenfunctions of the Γ_6 doublets, and INS intensity was only observed for the $\Gamma_5 \rightarrow \Gamma_6^{(1)}$ transition at elevated temperature, it is hard to judge this discrepancy at the moment. We have also found that these differences do not qualitatively affect the calculated thermodynamic properties at temperatures below 50 K.

As shown in Table V, for NdPd_2Al_3 all five calculated CF levels have the same order as the CF level sequence reported in Ref. 7. Even though our calculated eigenenergies and wave function coefficients differ somewhat from the reported values (e.g., the calculated eigenvalue of the second lowest level is two times larger than the reported value), the differences of the eigenvalues between the neighboring levels (transition energies of the INS) are comparable with the measured data. As pointed out by Dönni *et al.*,⁶ the physical properties of NdPd_2Al_3 are dependent on sample preparation procedures, and the authors have only done powder neutron scattering experiments on NdPd_2Al_3 and partially on PrPd_2Al_3 .

Table VI exhibits the calculated crystal field parameters and states together with rescaled data provided by Dönni

TABLE V. CF parameters B_{lm} (meV), eigenfunctions Γ_ν , and eigenenergies ε_ν (meV) of NdPd_2Al_3 calculated by DF-CFT in comparison with the experimental (INS or fitted) data of Ref. 7.

B_{lm} (this work)		B_{lm} (Ref. 7)		
B_{20}	0.278	B_{20}	0.214 ± 0.005	
B_{40}	-0.145×10^{-2}	B_{40}	$(-0.105 \pm 0.002) \times 10^{-2}$	
B_{60}	-0.114×10^{-4}	B_{60}	$(-0.224 \pm 0.006) \times 10^{-4}$	
B_{66}	0.116×10^{-2}	B_{66}	$(0.438 \pm 0.021) \times 10^{-3}$	
Γ_ν (this work)	ε_ν	Γ_ν (Ref. 7)	ε_ν	
$\Gamma_8^{(2)}$	$0.498 \pm \frac{5}{2}\rangle + 0.867 \mp \frac{7}{2}\rangle$	$\Gamma_8^{(2)}$	$0.288 \pm \frac{5}{2}\rangle + 0.958 \mp \frac{7}{2}\rangle$	12.24 ± 0.15^a
$\Gamma_9^{(2)}$	$0.257 \pm \frac{3}{2}\rangle + 0.996 \mp \frac{9}{2}\rangle$	$\Gamma_9^{(2)}$	$0.133 \pm \frac{3}{2}\rangle + 0.991 \mp \frac{9}{2}\rangle$	11.8 ± 0.3
$\Gamma_8^{(1)}$	$0.867 \pm \frac{5}{2}\rangle - 0.498 \mp \frac{7}{2}\rangle$	$\Gamma_8^{(1)}$	$0.958 \pm \frac{5}{2}\rangle - 0.288 \mp \frac{7}{2}\rangle$	4.24 ± 0.05^a
$\Gamma_9^{(1)}$	$0.996 \pm \frac{3}{2}\rangle - 0.257 \mp \frac{9}{2}\rangle$	$\Gamma_9^{(1)}$	$0.991 \pm \frac{3}{2}\rangle - 0.133 \mp \frac{9}{2}\rangle$	0.83 ± 0.03^a
Γ_7	$ \pm \frac{1}{2}\rangle$	Γ_7	$ \pm \frac{1}{2}\rangle$	0

^aINS data.

TABLE VI. CF parameters B_{lm} (meV), eigenfunctions Γ_ν , and eigenenergies ε_ν (meV) of PrPd_2Ga_3 calculated by DF-CFT in comparison with the experimental (INS) or fitted and extrapolated data of Ref. 9.

B_{lm} (this work)		B_{lm} (Ref. 9)	
B_{20}	0.924	B_{20}	0.828 ± 0.018
B_{40}	-0.428×10^{-2}	B_{40}	$(-0.297 \pm 0.006) \times 10^{-2}$
B_{60}	0.635×10^{-4}	B_{60}	$(0.304 \pm 0.008) \times 10^{-4}$
B_{66}	-0.318×10^{-2}	B_{66}	$(-0.619 \pm 0.031) \times 10^{-3}$
Γ_ν (this work)		Γ_ν (Ref. 9)	
	ε_ν		ε_ν
$\Gamma_6^{(2)}$	$-0.220 \pm 2\rangle + 0.975 \mp 4\rangle$	$\Gamma_6^{(2)}$	$0.048 \pm 2\rangle - 0.999 \mp 4\rangle$
Γ_4	$0.707 +3\rangle - 0.707 -3\rangle$	Γ_4	$0.707 +3\rangle - 0.707 -3\rangle$
Γ_3	$0.707 +3\rangle + 0.707 -3\rangle$	Γ_3	$0.707 +3\rangle + 0.707 -3\rangle$
$\Gamma_6^{(1)}$	$0.975 \pm 2\rangle + 0.220 \mp 4\rangle$	$\Gamma_6^{(1)}$	$0.999 \pm 2\rangle + 0.048 \mp 4\rangle$
Γ_5	$ \pm 1\rangle$	Γ_5	$ \pm 1\rangle$
Γ_1	$ 0\rangle$	Γ_1	$ 0\rangle$
	48.7		41.4 \pm 0.8
	43.2		31.0 \pm 0.4
	27.2		27.9 \pm 0.3
	20.5		16.57 \pm 0.04 ^a
	6.8		5.2 \pm 0.01 ^a
	0		0

^aINS data.

*et al.*⁹ for PrPd_2Ga_3 . It can be seen that all our calculated parameters have the same sign and similar magnitudes as the results given in Ref. 9, and the calculated crystal levels have the same sequence as the extrapolated levels. The low temperature INS experiment (at $T=15$ K) again provides only the energy 5.2 meV of the first excited CF state (Γ_5 doublet). At higher temperature, $T=40$ K, a peak corresponding to the $\Gamma_5 \rightarrow \Gamma_6^{(1)}$ CF excitation is observed at 11.4 meV, which is slightly higher than the corresponding excitation on the PrPd_2Al_3 compound. The energies of both measured excitations are reasonably well reproduced in our calculations. The extrapolated complete spectrum of the 3H_4 multiplet is broader than that of the PrPd_2Al_3 compound. Such a trend is obtained in our density functional calculations as well.

Table VII shows the comparison between the calculated CF parameters B_{lm} , eigenfunctions Γ_i , and eigenenergies ε_i with the fitted or observed results for NdPd_2Ga_3 .⁹ For this compound the observed transition energy between the ground state Γ_7 and the first excited level $\Gamma_9^{(1)}$ amounts to 18 K. Our calculations yield a similar energy separation 19 K but the ground state and the two lowermost excited levels are

interchanged. This apparent contradiction does not much affect the magnetic susceptibility and the magnetic specific heat in the temperature range $T > 30$ K, since they are determined by the lowest three CF levels in common. However, it influences the magnetic and thermodynamic behavior of the compound below T_N , especially the magnitude and the direction of the ordered magnetic moment.

Experimental data on the specific heat are available for all of the considered compounds except PrPd_2Al_3 . We will skip the latter compound and concentrate on the magnetic contribution c_m according to Eq. (12) for the remaining systems. Experimental information on c_m was obtained by subtracting the specific heat of the related La compound.^{6,8,34} The value of $J(\mathbf{q})^{\text{Nd}}$ was adjusted to 10.6 and 15.3 K for NdPd_2Al_3 and NdPd_2Ga_3 , respectively, to reproduce the measured critical temperatures.

Figure 3 shows the magnetic part of specific heat for NdPd_2Al_3 .⁶ The typical λ shape of the experimental curve is quite nicely obtained in the calculation as well. Only small differences between our calculated and the measured data can be observed above the critical temperature, possibly due

TABLE VII. CF parameters B_{lm} (meV), eigenfunctions Γ_ν , and eigenenergies ε_ν (meV) of NdPd_2Ga_3 calculated by DF-CFT in comparison with the experimental (INS or fitted) data of Ref. 9.

B_{lm} (this work)		B_{lm} (Ref. 9)	
B_{20}	0.317	B_{20}	0.234 ± 0.005
B_{40}	-0.107×10^{-2}	B_{40}	$(-0.100 \pm 0.002) \times 10^{-2}$
B_{60}	-0.506×10^{-4}	B_{60}	$(-0.149 \pm 0.004) \times 10^{-4}$
B_{66}	0.174×10^{-2}	B_{66}	$(0.303 \pm 0.015) \times 10^{-3}$
Γ_ν (this work)		Γ_ν (Ref. 9)	
	ε_ν		ε_ν
$\Gamma_8^{(2)}$	$0.476 \pm \frac{5}{2}\rangle + 0.880 \mp \frac{7}{2}\rangle$	$\Gamma_9^{(2)}$	$0.085 \pm \frac{3}{2}\rangle + 0.996 \mp \frac{9}{2}\rangle$
$\Gamma_9^{(2)}$	$0.299 \pm \frac{3}{2}\rangle + 0.954 \mp \frac{9}{2}\rangle$	$\Gamma_8^{(2)}$	$0.227 \pm \frac{5}{2}\rangle + 0.974 \mp \frac{7}{2}\rangle$
Γ_7	$ \pm \frac{1}{2}\rangle$	$\Gamma_8^{(1)}$	$0.974 \pm \frac{5}{2}\rangle - 0.227 \mp \frac{7}{2}\rangle$
$\Gamma_8^{(1)}$	$0.880 \pm \frac{5}{2}\rangle - 0.476 \mp \frac{7}{2}\rangle$	$\Gamma_9^{(1)}$	$0.996 \pm \frac{3}{2}\rangle - 0.085 \mp \frac{9}{2}\rangle$
$\Gamma_9^{(1)}$	$0.954 \pm \frac{3}{2}\rangle - 0.299 \mp \frac{9}{2}\rangle$	Γ_7	$ \pm \frac{1}{2}\rangle$
	22.6		13.3 \pm 0.3
	20.2		12.37 \pm 0.14 ^a
	2.1		5.45 \pm 0.04 ^a
	1.6		1.53 \pm 0.02 ^a
	0		0

^aINS data.

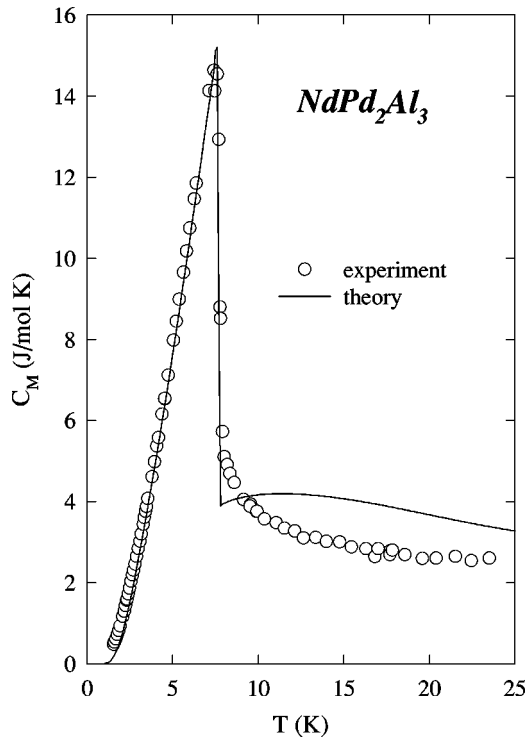


FIG. 3. Calculated and measured magnetic contributions to the specific heat of NdPd_2Al_3 . Solid line: DF-CFT calculation; circles: experiment (Ref. 6). Parameter used in the calculation: $J(\mathbf{q}) = 10.6$ K.

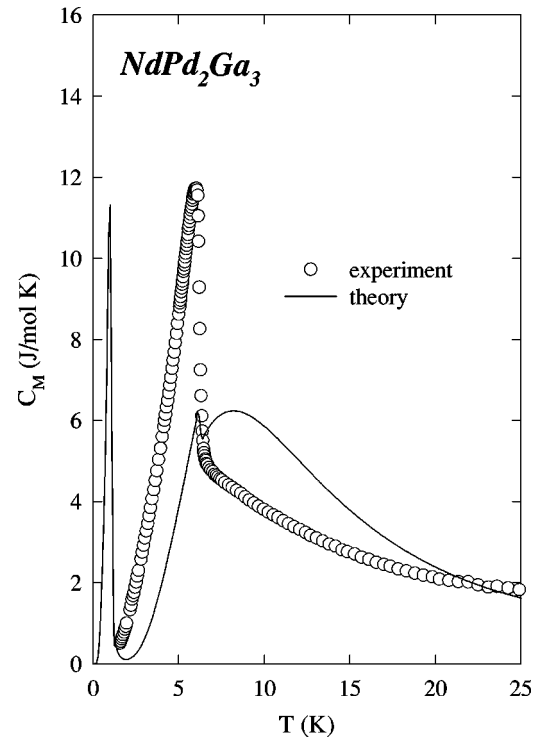


FIG. 4. Calculated and measured magnetic contributions to the specific heat of NdPd_2Ga_3 . Solid line: DF-CFT calculation; circles: experiment (Refs. 8,34). Parameter used in the calculation: $J(\mathbf{q}) = 15.3$ K.

to critical fluctuation not taken into account in our simple approach. The general good agreement demonstrates that the effective mean-field theory is sufficient to describe the low-temperature magnetic specific heat for the considered class of systems. In the case of NdPd_2Al_3 , the CF level sequence obtained from DFT calculations coincides with the experimental sequence, and this fact allows us to describe the quite complicated structure of c_m with only one free parameter.

The situation is different for the isostructural compound NdPd_2Ga_3 , where the calculated level sequence deviates from the experimental sequence (Table VII). The related energy differences are smaller than 10 meV, and the cross features of the level scheme (total splitting, three low-lying doublets and two high-lying doublets) are preserved. Anyhow, the wrong order of the calculated levels makes the calculated specific heat hard to compare with experiment,^{8,34} see Fig. 4. (Note that the additional low-temperature peak in the calculated curve originates from a crossing of the CF levels.) In order to demonstrate that the mean-field model is nonetheless applicable, we have calculated the magnetic specific heat for this substance with the CF parameter set obtained from experiment (Fig. 5). Here, as in the former substance, the gross agreement is good. Above a temperature of 10 K, however, a deviation between experimental and theoretical data is present that grows with temperature. A probable reason for this deviation is that the determination of the experimental magnetic specific heat as difference between two measured data sets might become less reliable for elevated temperature. In particular, the assumption that the phonon contribution in the lanthanum compound is the same as in the isostructural neodymium (or praseodymium) compound, worsens with rising weight of the phonon contribution with

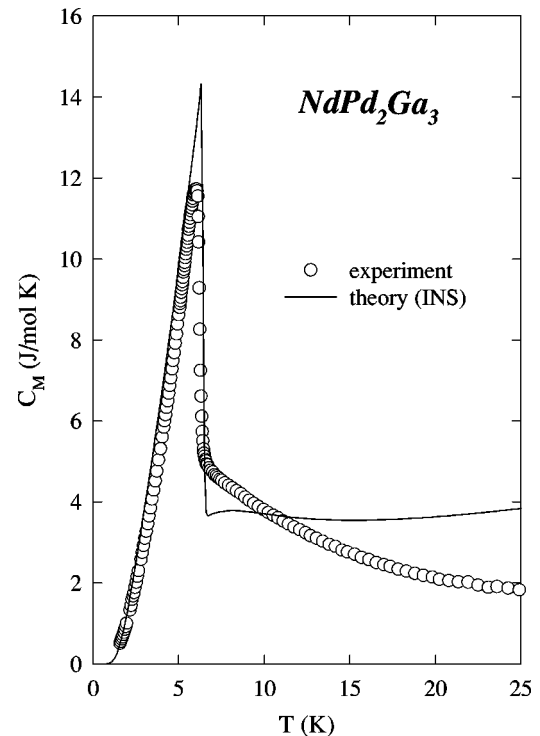


FIG. 5. Calculated and measured magnetic contributions to the specific heat of NdPd_2Ga_3 . Solid line: calculation; circles: experiment (Refs. 8,34). Parameter used in the calculation: CF parameters from INS data (Ref. 9) and $J(\mathbf{q}) = 15.3$ K.

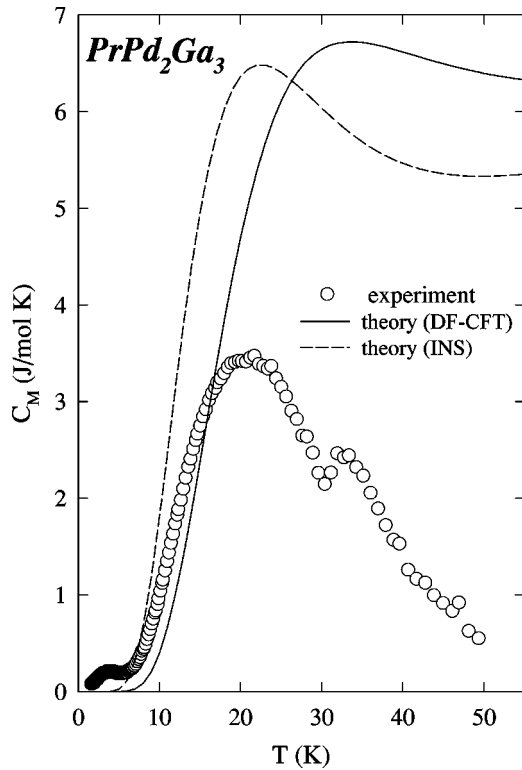


FIG. 6. Calculated and measured magnetic contributions to the specific heat of PrPd_2Ga_3 . Solid line: DF-CFT calculation; dashed line: calculation with CF parameters, rescaled from INS data (Ref. 9); circles: experiment (Refs. 8,34).

respect to the magnetic contribution to the specific heat. This point of view is supported by the data presented in Fig. 6, where the experimental values of c_m on PrPd_2Ga_3 (Refs. 8,34) are compared with the results of two calculations, using CF parameters from DF calculations and from fitting and extrapolating neutron data, respectively (both sets compiled in Table VI). In this case, experimental data are available up to 50 K, and the growing disparity between theoretical and experimental curves is clearly seen. Note, that the size of the difference at 30 K is quite similar to that in the previous system, see Fig. 5. It is clear that the almost vanishing “experimental” value of c_m at 50 K is not consistent with the observed CF level at 16.6 meV. Again, the most probable explanation of the inconsistency is a different phonon contribution to the specific heat of LaPd_2Ga_3 and PrPd_2Ga_3 .

Turning our attention to the paramagnetic susceptibilities, we note that only for NdPd_2Al_3 experimental data on a single crystalline sample are available.⁷ For the three remaining compounds, the susceptibility has been measured on polycrystalline samples, and quantitative experimental information on the anisotropy of χ is not available. We shall present our data on χ_{\parallel} and χ_{\perp} together with the averaged value in all these cases anyway, providing a theoretical prediction for future studies on single crystals. Figure 7 shows the related data for the system PrPd_2Al_3 . The calculated averaged susceptibility is larger than the measured one⁴ in the whole temperature range. At low temperatures where only the ground state singlet is thermally populated, half of the deviation is explained by the fact that the first excited CF level obtained from the DFT calculation is lower in comparison to the experimental level. The remaining small discrep-

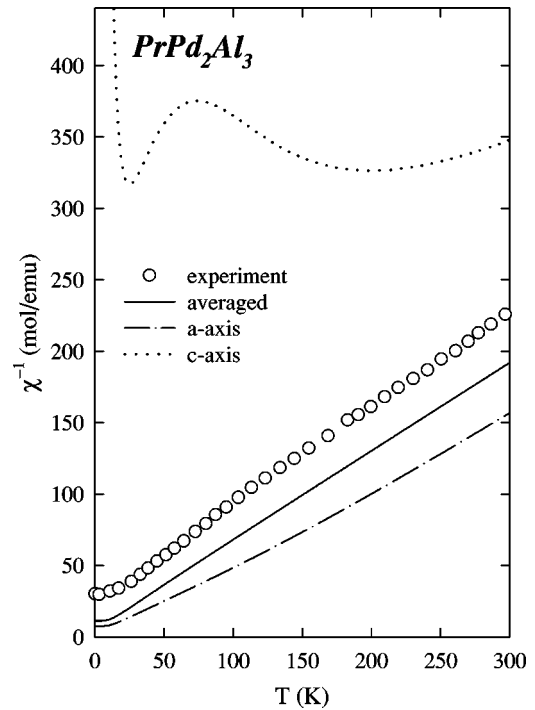


FIG. 7. Comparison between the calculated and measured inverse susceptibilities of PrPd_2Al_3 . DF-CFT calculations: solid line (averaged χ), dash-dotted line (χ_{\perp}), and dotted line (χ_{\parallel}); experiment: (Ref. 4) circles. Computed values of $\chi_P = 7.6 \times 10^{-5}$ emu/mol and $J_{f-c}(0)D(E_F) = 0.025$ are used.

ancy can be attributed to the neglect of the unknown molecular field, or to a nonideal texture of the polycrystalline sample.

For NdPd_2Al_3 , presented in Fig. 8, the calculated perpendicular susceptibility is almost perfectly matching the experimental curve.⁷ Experimental and theoretical curves of the susceptibility for the applied field parallel to the hexagonal axis exhibit the same shape and tendency, but the anisotropy in the susceptibility is overestimated in our calculation by about 50%. This is mainly due to the somewhat too large gross CF splitting found in the DFT-based calculation. The experimentally based CF parameters in this case do reproduce the measured susceptibilities very well. Thus, we can consider the present case as a typical example of what degree of quantitative coincidence between experimental data and parameter-free DF-CFT calculations can be expected.

Good agreement is found between the averaged measured⁸ and calculated susceptibilities of PrPd_2Ga_3 , see Fig. 9. A similar picture is found in the case of NdPd_2Ga_3 , Fig. 10. Here, we compare the calculated averaged susceptibility with unpublished experimental data, since the original measurement⁸ was improved later by the same group.¹¹ Again, we can consider our calculated data on the anisotropic susceptibilities as a prediction to be checked in future experiments.

V. CONCLUSIONS

A new variant of self-interaction corrected local spin-density theory has been combined with single-ion model calculations and applied to the class of rare-earth compounds RPd_2X_3 ($R = \text{Pr, Nd}$; $X = \text{Al, Ga}$). Our calculations are free

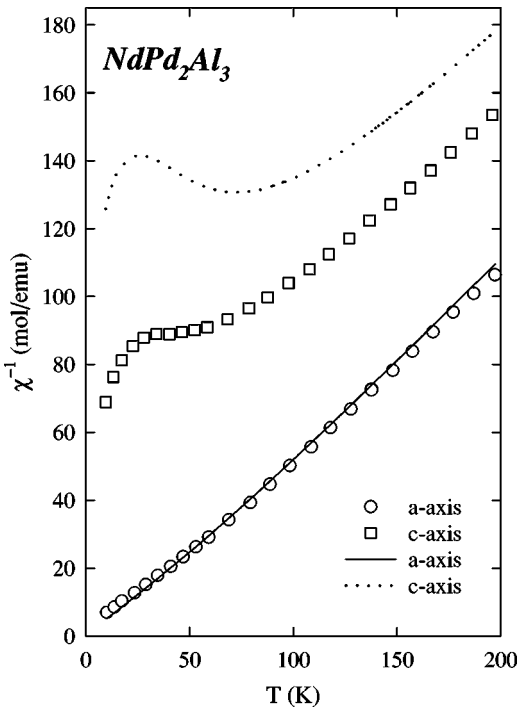


FIG. 8. Comparison between the calculated and measured inverse susceptibilities of NdPd_2Al_3 . DF-CFT calculations: solid line (χ_{\perp}) and dotted line (χ_{\parallel}); experiment: (Ref. 7) circles (χ_{\perp}) and squares (χ_{\parallel}). Computed values of $\chi_P = 7.6 \times 10^{-5}$ emu/mol and $J_{f-c}(0)D(E_F) = 0.026$ are used.

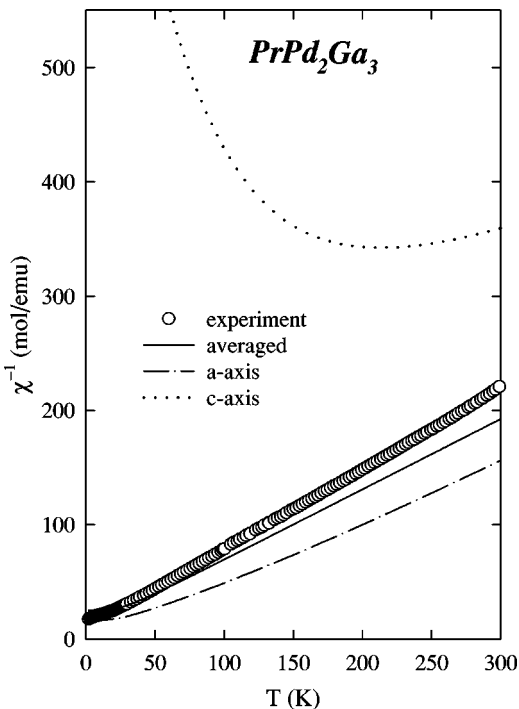


FIG. 9. Comparison between the calculated and measured inverse susceptibilities of PrPd_2Ga_3 . DF-CFT calculations: solid line (averaged χ), dash-dotted line (χ_{\perp}), and dotted line (χ_{\parallel}); experiment: (Ref. 8) circles. Computed values of $\chi_P = 6.2 \times 10^{-5}$ emu/mol and $J_{f-c}(0)D(E_F) = 0.022$ are used.

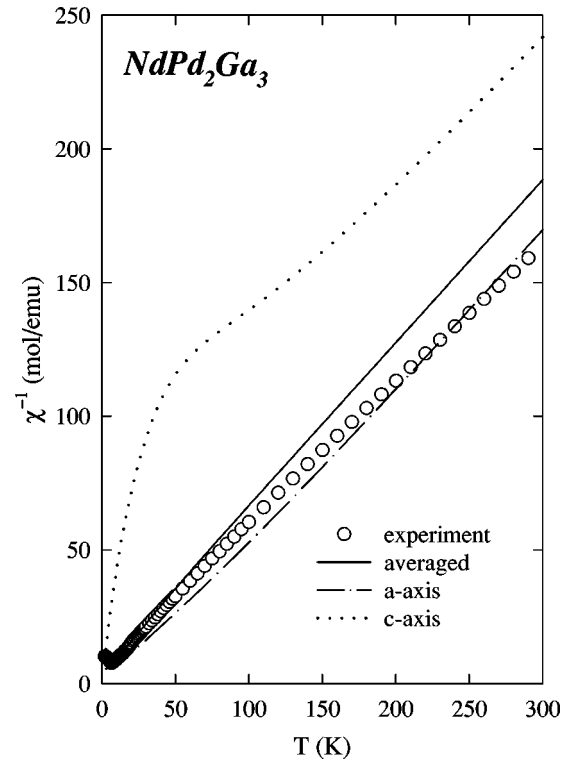


FIG. 10. Comparison between the calculated and measured inverse susceptibilities of NdPd_2Ga_3 . DF-CFT calculations: solid line (averaged χ), dash-dotted line (χ_{\perp}), and dotted line (χ_{\parallel}); experiment: (Ref. 11) circles. Computed values of $\chi_P = 6.7 \times 10^{-5}$ emu/mol and $J_{f-c}(0)D(E_F) = 0.020$ are used.

of adjustable parameters except the strength of isotropic molecular field interaction that is adjusted to reproduce the experimental value of the Néel temperature in the Nd compounds. Satisfactory agreement with CF parameters from literature is found, in particular for the second and fourth order parameters. The calculated CF levels, paramagnetic susceptibilities and specific heats of the considered compounds are close to available experimental data. In particular, this agreement is improved by taking into account the intra-atomic spin correlations within the $4f$ shell when calculating the $4f$ orbital density.

The anisotropic susceptibility is predicted for three different compounds and compared to existing single-crystal data on NdPd_2Al_3 . Further experimental work on single crystal-line samples could help to improve our present understanding of the crystal field properties of the considered systems.

Our results demonstrate that single-ion model calculations with crystal field parameters obtained from density functional theory are well applicable to compounds of rare earth elements with nonmagnetic metals. This was not the case for the isostructural system UPd_2Al_3 , where large discrepancies between experimental and theoretical data on susceptibility and specific heat were found.¹³

ACKNOWLEDGMENTS

We wish to thank M. Kuz'min for valuable discussions, as well as H. Kitazawa and E. Bauer for sending us preprints and experimental data prior to publication. E. Bauer, H. Kitazawa, and A. Dönni kindly allowed us to present unpub-

lished experimental data. We are grateful to the Max-Planck Society for financial support. Further, support by the Bundesministerium für Bildung und Forschung der Bundesrepublik Deutschland (BMBF, Projekt 13N6612/4) and by

the Deutsche Forschungsgemeinschaft (SFB 463, TP B2) is gratefully acknowledged. The work of M.D. was supported by the Grant Agency of the Czech Republic under Grant Nos. 202/99/0184 and 106/98/0507, respectively.

- ¹C. Geibel, C. Schank, S. Thies, H. Kitazawa, C. D. Bredl, A. Bohm, M. Rau, A. Grauel, R. Caspary, R. Helfrich, U. Ahlheim, G. Weber, and F. Steglich, *Z. Phys. B* **84**, 1 (1991).
- ²A. Krimmel, P. Fischer, B. Roessli, H. Maletta, C. Schank, A. Grauel, A. Loidl, and F. Steglich, *Z. Phys. B* **86**, 161 (1992).
- ³H. Kitazawa, C. Schank, S. Thies, B. Seidel, C. Geibel, and F. Steglich, *J. Phys. Soc. Jpn.* **61**, 1461 (1992).
- ⁴K. Ghosh, S. Ramakrishnan, S. K. Malik, and Girish Chandra, *Phys. Rev. B* **48**, 6249 (1993).
- ⁵H. Kitazawa, A. Mori, S. Takano, T. Yamadaya, A. Matsushita, and T. Matsumoto, *Physica B* **186-188**, 661 (1993).
- ⁶A. Dönni, H. Kitazawa, P. Fischer, T. Vogt, A. Matsushita, Y. Iimura, and M. Zolliker, *J. Solid State Chem.* **127**, 169 (1996).
- ⁷A. Dönni, A. Furrer, H. Kitazawa, and M. Zolliker, *J. Phys.: Condens. Matter* **9**, 5921 (1997).
- ⁸E. Bauer, M. Liendl, L. Naber, D. Werner, H. Michor, G. Hilscher, A. Dönni, P. Fischer, F. Fauth, and M. Zolliker, *Z. Phys. B* **102**, 291 (1997).
- ⁹A. Dönni, A. Furrer, B. Bauer, H. Kitazawa, and M. Zolliker, *J. Phys. B* **104**, 403 (1997).
- ¹⁰Y. Shimizu and O. Sakai, *J. Phys. Soc. Jpn.* **65**, 2632 (1996).
- ¹¹A. Dönni *et al.* (unpublished).
- ¹²M. Diviš, M. Richter, H. Eschrig, and L. Steinbeck, *Phys. Rev. B* **53**, 9658 (1996).
- ¹³M. Richter, M. Diviš, J. Forstreuter, K. Koepernik, L. Steinbeck, and H. Eschrig, *Physica B* **230-232**, 519 (1997).
- ¹⁴D. Gignoux and D. Schmitt, in *Handbook of Magnetic Materials*, edited by K. H. J. Buschow (North-Holland, Amsterdam, 1997), Vol. 10, pp. 239–413.
- ¹⁵A. M. Stewart, *Phys. Rev. B* **6**, 1985 (1972).
- ¹⁶We made use of the scalar relativistic linear combination of atomic orbitals method, see Refs. 25,26.
- ¹⁷M. S. S. Brooks, L. Nordström, and B. Johansson, *J. Phys.: Condens. Matter* **3**, 2357 (1991).
- ¹⁸M. S. S. Brooks, L. Nordström, and B. Johansson, *J. Phys.: Condens. Matter* **3**, 3393 (1991).
- ¹⁹M. T. Hutchings, *Solid State Phys.* **16**, 227 (1964).
- ²⁰K. W. H. Stevens, *Proc. Phys. Soc. London, Sect. A* **65**, 209 (1952).
- ²¹U. von Barth and L. Hedin, *J. Phys. C* **5**, 1629 (1972).
- ²²J. P. Perdew and A. Zunger, *Phys. Rev. B* **23**, 5048 (1981).
- ²³A. Svane, *Phys. Rev. B* **53**, 4275 (1996).
- ²⁴M. Richter, *J. Phys. D* **31**, 1017 (1998).
- ²⁵M. Richter, P. M. Oppeneer, H. Eschrig, and B. Johansson, *Phys. Rev. B* **46**, 13 919 (1992).
- ²⁶H. Eschrig, *Optimized LCAO Method and the Electronic Structure of Extended Systems* (Springer-Verlag, Berlin, 1989).
- ²⁷L. Steinbeck, M. Richter, H. Eschrig, and U. Nitzsche, *Phys. Rev. B* **49**, 16 289 (1994).
- ²⁸M. Richter *et al.*, *J. Alloys Compd.* **225**, 469 (1995).
- ²⁹L. Steinbeck, M. Richter, U. Nitzsche, and H. Eschrig, *Phys. Rev. B* **53**, 7111 (1996).
- ³⁰M. Diviš, M. Richter, J. Forstreuter, K. Koepernik, and H. Eschrig, *J. Magn. Magn. Mater.* **176**, L81 (1997).
- ³¹T. Oguchi, K. Terakura, and M. Hamada, *J. Phys. F* **13**, 145 (1983).
- ³²A. J. Pindor, J. Staunton, G. M. Stocks, and H. Winter, *J. Phys. F* **13**, 979 (1983).
- ³³Such calculations on the paramagnetic state of Gd metal were recently reported by L. M. Sandratskii and J. Kubler, in *Magnetism and Electronic Correlations in Local-Moment Systems: Rare-Earth Elements and Compounds* edited by M. Donath, P. A. Dowben, and W. Nolting (World Scientific, Singapore, 1998) p. 271.
- ³⁴E. Bauer (unpublished).